



Investigations on the process window for friction stir assisted double-sided incremental forming with synchronous bonding of steel and aluminum alloy sheets

Renhao Wu^{1,2} · Xinmei Liu^{1,2} · Meng Li^{1,2} · Jun Chen^{1,2}

Received: 14 April 2021 / Accepted: 10 January 2022 / Published online: 27 January 2022
© The Author(s), under exclusive licence to Springer-Verlag France SAS, part of Springer Nature 2022

Abstract

Dissimilar steel/Al laminates are more widely utilized in lightweight and anti-vibration structures while the preparation and forming processes remain challenging due to obvious difference in materials properties. In this work, separated DC05 and AA5052-H32 sheets are used to fabricate truncated conical laminated parts by a novel pin-less friction stir assisted double-sided incremental forming with synchronous bonding process. The peeling force of formed parts as a metric of bonding strength is evaluated to obtain parameters window based on response surface method. The effects of step down, rotation speed of master tool, wall angle, and their cross terms on bonding strength are investigated. The present work established a functional model to determine optimal parameter combination for better bonding strength. Working temperature and forming force are consistent through process evolution. Optimal solution is also conducted to obtain ultimate forming depth and better surface finish of truncated parts. The findings in this work can help deeply understand the fabrication procedures and thermomechanical results in dissimilar bonding-with-forming processes.

Keywords Aluminum alloy/steel dissimilar bonding · Friction stir · Incremental plastic deformation · Process window · Forming performance

Introduction

The emerging requirements of dissimilar laminates with lightweight structures and high energy consumption in industries are stimulating rapid development. In recent years, Al-steel hybrid structures have been recognized to effectively

applied in industrial products [1]. However, achieving sound bonding quality remains an intensively technological challenge owing to the distinct thermomechanical property differences between the materials [2], especially for Al/steel joints. The formation of brittle intermetallic compounds (IMCs) at the interface cause great limitation for subsequent plastic deformation, which may easily lead to crack [3].

To overcome the drawbacks of interfacial micro voids and brittle IMCs and increase the static and fatigue performance, various solid-state bonding processes are developed [4–8]. Many derivative preparation processes are based on the principle of friction stir welding (FSW). As reviewed by Mishra and Ma [9], heat is generated by friction between rotation tool and the plates during FSW process which also involves severe plastic deformation. FSW-related solid-state bonding processes can produce smaller heat-affected zone and better performance than other welding technologies and has been regarded as a promising approach for joining dissimilar sheets. To suppress the formation of brittle IMC phase and obtain better bonding quality, Liu et al. [10] reported that

Renhao Wu and Xinmei Liu contributed equally to this work.

This article belongs to the Topical Collection: Developments in modelling and simulation of material forming, a focus on Japan, South Korea and China.

✉ Jun Chen
jun_chen@sjtu.edu.cn

¹ Department of Plasticity Technology, School of Materials Science and Engineering, Shanghai Jiao Tong University, Shanghai 200030, China

² National Engineering Research Center of Die & Mold CAD, School of Materials Science and Engineering, Shanghai Jiao Tong University, 200030 Shanghai, China

thickness of IMC can be controlled by carefully designed FSW conditions. Nevertheless, some drawbacks such as undesirable ‘keyhole-channel’ defects left at the end of weld line, severe wear of tool pin, and high axial forming force leave negative roles on bonding strength and equipment stiffness. Therefore, pin-less FSW processes [11–13] are developed to overcome the drawbacks and produce sound joints with metallurgical reaction interfaces. Moreover, investigations on dissimilar joining process also indicate that plastic deformation shows positive role in interfacial bonding [14]. Zhao et al. [15] and Liu et al. [16] conducted numerical and experimental works on heat generation and material flow in ultrasonic assisted friction stir welding (UaFSW), which reveal that plastic deformation can reduce loading force significantly. To reveal the dependency from the process parameters on axial processing forces and temperature distribution in bonding area, D’Urso and Giardini [17] established a heat-force coupled finite element model to study the thermomechanical effect on FSW joints.

Incremental sheet forming (ISF) process has been developed for decades, which can achieve high formability for ductile sheets attributed to its cyclic local loading features as clarified by Jackson and Allwood [18]. Emmens et al. [19] and Cerro et al. [20] conducted deep investigations on the effects of common process parameters such as step down, wall angle, sheet thickness, and tool radius on formability. Moreover, Lu et al. [21] revealed that double-sided incremental forming process can increase formability for the lower stress triaxiality in the existed compressive-squeeze area. Some heat-input procedures were employed in ISF-related processes [22–24] to further improve higher formability for aluminum alloy and other low-ductility sheets. Among the hot ISF processes, friction stir assisted solution is more efficient attributed to high-speed rotational tool, which also possesses the good potential to combine with pin-less FSW process.

Obviously, progresses of FSW and ISF related processes encourage the development of dissimilar solid-state bonding with deformation technologies. However, Al/steel bonding with overall plastic deformation remains few reports. Matsumoto et al. [25] employed friction stir incremental deformation process to achieve incremental joining of open-cell nickel foam and polymethyl methacrylate sheet, which leads almost global plastic deformation on base materials. Following similar principle, Li et al. [26, 27] proposed a novel pin-less friction stir assisted incremental sheet forming with synchronous bonding (FS-ISF&SB) process to complete AA5052-H32/DC05 dissimilar bonding with overall plastic deformation. Then Cai et al. [28] conducted simulation study to validate heat-force conditions and interfacial contact behaviors with the experimental phenomenon of this process.

In the present work, a modified friction stir assisted double-sided incremental forming with synchronous bonding (FS-DSIF&SB) process is utilized with the advent of FS-ISF&SB process to better solve the issues of overall plastic deformation with synchronous dissimilar bonding in industrial productions. Experimental procedures are briefly introduced. Then process window is established and tested by peeling experiments. Optimal parameters combination is also derived and validated. Forming performances of optimal solution in ultimate forming depth and surface finish quality are discussed. Finally, some concluding remarks are summarized.

Experimental procedures

FS-DSIF&SB system

The self-built forming system is displayed in Fig. 1(a), which is mainly composed of CNC control system and temperature-force detection system. Infrared camera (thermoIMAGER 160) is used to capture the temperature history through the process, especially peak temperature in localized loading area. As-received DC05 and AA5052-H32 sheets are fixed together on the clamping system in same rolling direction.

As illustrated in Fig. 1(b), the high-speed rotational master tool (MT) performs local loading with friction heat while slave tool (ST) moves coordinately and provides adequate back pressure by preset spiral toolpath. The rigid tools are flat-bottomed and rounded which ensure the dissimilar sheets to steadily deform. With the cyclic thermomechanical effects, the localized materials can be bonded with incremental deformation. The parameters in this flexible processing configuration can be adjusted according to specific materials or forming requirements to achieve different frictional heat input conditions.

Materials preparation

AA5052-H32 as outer sheet with thickness of 1.0 mm and steel DC05 as inner sheet with thickness of 0.8 mm are cut in a size of 180 mm x 180 mm. Nominal chemical composition and mechanical properties of the as-received sheets are listed in Tables 1 and 2.

To ensure interfacial bonding strength, the contact surfaces of the dissimilar sheets are polished by electric brush to remove oxide film. Electric brush is used to remove the oxide layer of the contacted surfaces. All surfaces are rinsed with alcohol to clean up debris and oil. The outer side of AA5052 is evenly sprayed with high temperature resistant black paint and lubricant.

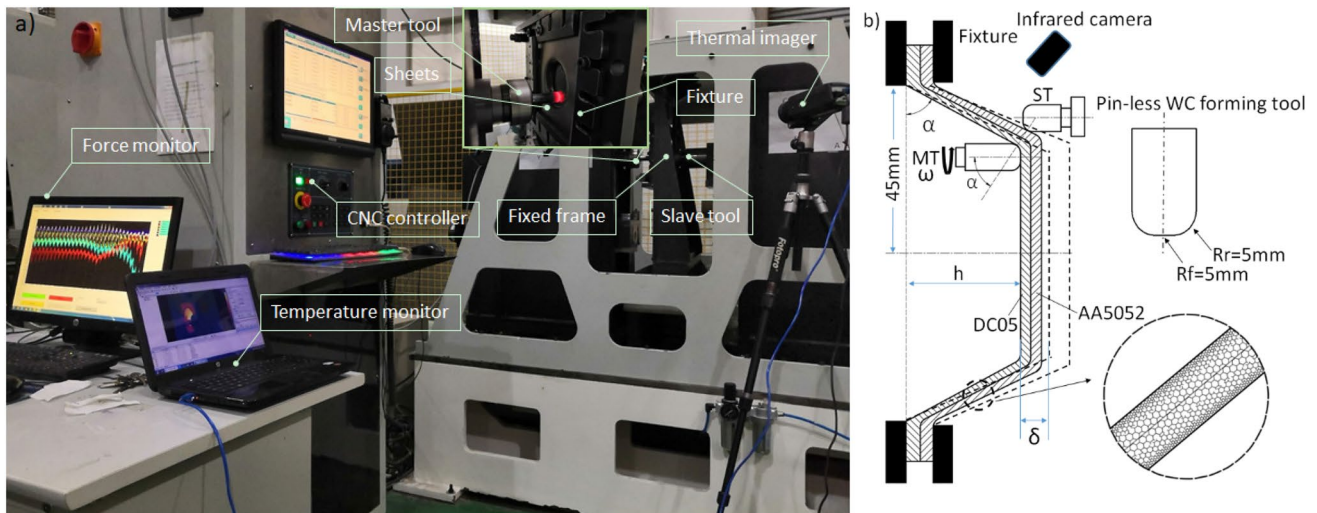


Fig. 1 FS-DSIF&SB process: (a) experimental configure, (b) forming illustration

Table 1 Nominal chemical composition of as-received AA5052 and DC05 sheets (in wt%) [26]

Materials	C	P	S	Mg	Si	Fe	Mn	Cr	Others	Al
AA5052	--	--	--	2.2-2.8	0.25	0.4	0.1	0.15-0.35	0.35	Bal.
DC05	0.06	0.02	0.02	--	0.02	Bal.	0.35	--	--	0.01

Table 2 Mechanical properties of as-received AA5052 and DC05 sheets [26]

Materials	Density (g/cm ³)	Young's modulus (GPa)	Yield strength (MPa)	Melting temperature (°C)	Elongation at break (%)
AA5052	2.7	69	175	607	15
DC05	7.85	200	136	1500	33.9

Establishment of process window

Tests of process design

As a hybrid process combined with DSIF and pin-less FSW process, related parameters (most concern: step down δ , wall angle α , rotation speed of MT ω) require further clarification on their roles. Therefore, reasonable process window shall be validated through corresponding tests. Mathematic analysis software *Design Expert 10* is useful to set experimental plan for obtaining persuasive and comprehensive experimental results. Based on response surface methodology (RSM) with quadratic regression model [29], Central Composite Design (CCD) is chosen here. The advantage of CCD comes from its flexibility and usefulness as a sequential experimental design. As shown in Fig. 2(a), the choice of axial distance and the number of center points is adjustable. The selection of the axial

distance involves the design rotation, the robustness of the model, and the robustness of the parameter estimation extrapolation. The number of center points controls characteristics of CCD. The addition of center points holds the characteristics of orthogonality and the uniform precision design, which also ensures optimized value within defined unit distance.

Based on the previous work [26], step down δ , wall angle α , rotation speed of MT ω are selected to build proper process window. By setting and automatically adjusting parameters limits in a quadratic model of CCD, total 22 experiments are generated by Table 3. The details on parameters combination can also refer to Fig. 3. The test of center point is the key component of CCDs as the decisive factor to achieve consistent accuracy, which has been repeated for 8 times during a series of tests.

Central response surface method (C-RSM) as a solution of CCD is used to conduct experiments. The popularity of C-RSM can be attributed to the following aspects: (1) The sequential nature of C-RSM, which can be divided into two subsets, the first subset estimates linear and two-factor interaction effects, and the second estimates collective effects of curvature; (2) C-RSM provides details about experimental variables and errors with the least test numbers; (3) C-RSM is very flexible, and their design types can be applied to different operating and design domains. Therefore, C-RSM is widely used in engineering, scientific research and industry.

Table 3 Variable parameter levels by using quadratic model for CCD

Forming parameters	Given limits	Adjusted test limits	
Step down δ /mm	0.15~0.35	0.1~0.4	Target: Peeling force/N Non-center points: 14 Center points: 8 Span=1.5
Wall angle α /°	50~60	47.5~62.5	
Rotation speed of MT ω /RPM	2800~3600	2600~3800	

Fig. 2 Test design and fabricated laminated parts: (a) illustration of central composite design, (b) AA5052 side, (c) DC05 side, (d) peeling from intermetallic layer, PIMC, (e) no bonding, NB, (f) peeling from substrate material, PS

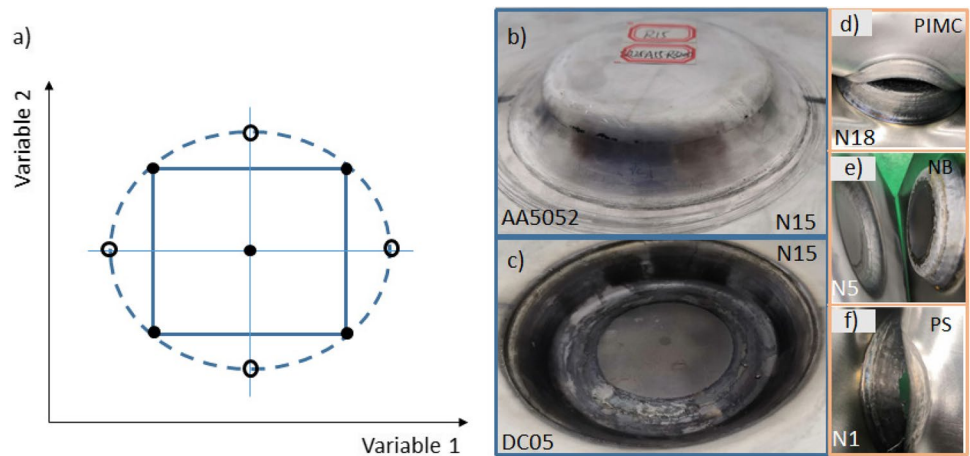
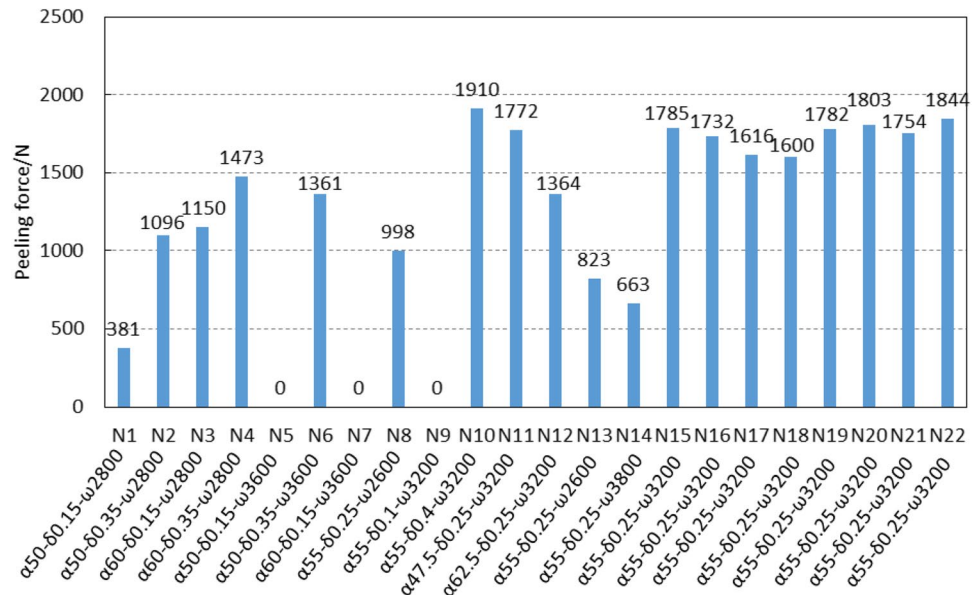


Fig. 3 Peeling force of each DC05/AA5052 laminated part fabricated by 22 FS-DSIF&SB tests



The optimal target of the process is the bonded strength. The adopted peeling method for testing the target of fabricated parts like Fig. 2(b)-(c) is introduced as follows. First, one of corners of the part is bent at 180°, and then fixed in the universal testing machine, pulled at speed of 5mm/s. The tensile load-displacement curve is recorded in real time to measure maximum peeling force. Through the peeling test, three different interfacial peeling modes are obtained

as shown in Fig. 2(d)-(f), namely peeling from IMC (PIMC), no bonding (NB), peeling from substrate material (PS).

The maximum peeling force is regarded as the target of bonding strength in C-RSM. The results of 22 tests (i.e., N1-N22) are shown in Fig. 3. In the tests N1, N5, N7, N9, peeling force of the NB mode is less than 500 N because the interface is only mechanically engaged or IMC is unstable that can be neglected. In the PIMC mode (N2, N3, N8,

N13, N14), the peeling force depends on IMC components and distribution. Therefore, in PS mode (N4, N6, N10, N11, N12, N15, N16, N17, N18, N19, N20, N21, N22), the peeling force of bonded interface is higher than the matrix, which demonstrates the optimal bond mode under the processing condition.

Target optimization model of interfacial bonding

According to C-RSM, a quadratic model is considered here to fit the process parameters.

$$y = \lambda_0 + \sum_{i=1}^n \lambda_i x_i + \sum_{i=1}^n \lambda_{ii} x_i^2 + \sum \sum \lambda_{ij} x_i x_j + \xi \tag{1}$$

Where ξ is the remaining item, λ is the slope of different sub terms. x, y are the process parameters and target peeling force, which can be defined from,

$$\begin{aligned} x \in E, y(x) \rightarrow \max \\ \lambda_i = \frac{\partial y}{\partial x_i} = 0 \quad (i = A, S, R; n = 1, 2) \\ \bar{x}_i \leq x_i \leq \underline{x}_i \quad (\bar{x}_i = \text{up limit of } E, \underline{x}_i = \text{low limit of } E) \end{aligned} \tag{2}$$

Regression analysis is performed according to the experimental results, and the least square method is used to estimate the bonded strength under different parameter combinations to construct a response surface. The functional relationship between the response target and the process parameters is obtained as Eq. (3). The coefficients are listed in Table 4.

$$y = \lambda_0 + \lambda_1 \delta + \lambda_2 \alpha + \lambda_3 \omega + \lambda_4 \delta \alpha + \lambda_5 \delta \omega + \lambda_6 \alpha \omega + \lambda_7 \delta^2 + \lambda_8 \alpha^2 + \lambda_9 \omega^2 \tag{3}$$

The difference between the predicted value of the regression equation and the actual test result and the residual normal probability distribution are shown in Fig. 4(a) and (b), respectively. The residual points fluctuate slightly near the diagonal, and the predicted maximum peeling force and actual test results are also near the diagonal of the first quadrant ($k=1$), which proves that the maximum peeling force predicted by the C-RSM model is in satisfactory reliability. As derived by Eq. (3), the optimal solution is that: $\delta=0.323\text{mm}$, $\alpha=53.379^\circ$, $\omega=3210.176\text{ RPM}$. Peeling force of fabricated part can reach 1925 N in this case.

Analysis of Variance (ANOVA) listed in Table 5 proves the higher fitting accuracy and applicability of the model. By analyzing the F and P values of each parameter and their cross terms, step down and rotation speed of MT occupy significant roles.

Additionally, according to the ANOVA results, significance level of the process parameters and their combinations can be derived as,

$$\delta > \omega^2 > \delta^2 > \omega > \alpha \omega > \delta \omega > \alpha^2 > \delta \alpha > \alpha \tag{4}$$

Table 4 The value of coefficient λ_0 - λ_9

λ_0	λ_1	λ_2	λ_3	λ_4	λ_5	λ_6	λ_7	λ_8	λ_9
1745.7	501.0	13.7	-158.5	-94.3	165.2	-188.6	-366.0	-93.6	-460.2

Fig. 4 (a) comparison of predicted and actual peeling force, (b) normal plot of residuals

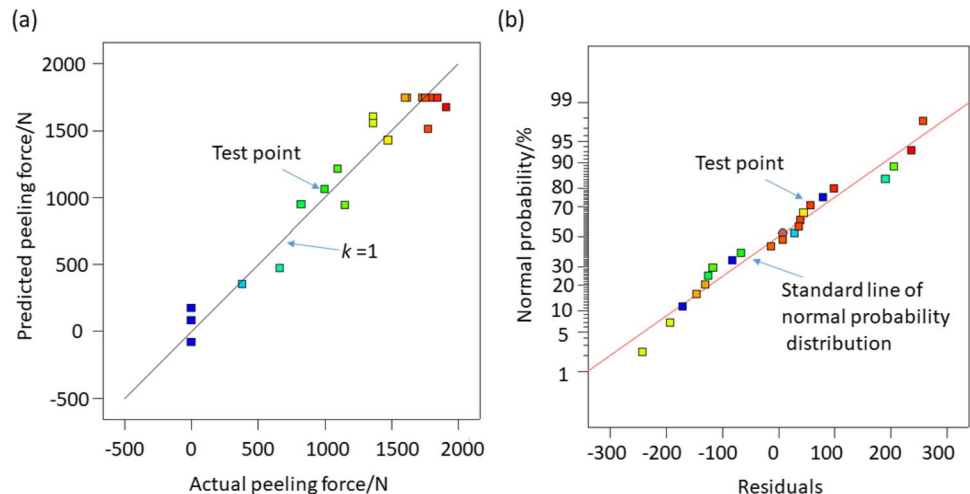


Table 5 The result of ANOVA

Items	Sum of squares	DOF	F	P Prob>F*	Degree of relevance
Fitted model	8.377E+006	9	26.08	<0.0001	Significant
δ -step down	3.317E+006	1	87.90	<0.0001	Significant
α -Wall angle	2344.76	1	0.066	0.8021	
ω -Rotation speed	3.139E+005	1	8.79	0.0118	
$\delta\alpha$	71158.78	1	1.99	0.1834	
$\delta\omega$	2.183E+005	1	6.12	0.0293	
$\alpha\omega$	2.845E+005	1	7.97	0.0154	
δ^2	1.458E+006	1	40.86	<0.0001	Significant
α^2	95386.12	1	2.67	0.1280	
ω^2	2.306E+006	1	64.61	<0.0001	Significant
Fitting R^2	0.9514				

*If $P>F$ less than 0.05, the degree of relevance can be considered as significant

Effects of process parameters on interfacial bonding

To concretely reveal the effects of process parameters on interfacial bonding, independent step down δ , wall angle α , and rotation speed of MT ω and their cross terms versus the maximum peeling force is represented by a contour map in Fig. 5.

Analyses in Table 5 and experimental results in Fig. 3 indicate that the interaction of various process parameters has a significant impact on the maximum peeling force.

As wall angle is fixed as 55° , the elliptical shape as shown in Fig. 5(a) indicates that the interaction between step down and rotation speed is obvious. When step down is 0.25-0.35mm and rotation speed is 3000-3400RPM, the maximum peeling force is greater than 1500 N.

As step down equals to 0.25mm, it can be seen from the interval of contour map as shown in Fig. 5(b) that the influence of the rotation speed on maximum peeling force is obviously greater than wall angle.

As rotation speed of MT is maintained at 3200RPM, if step down is large, maximum peeling force changes with wall angle more obviously as illustrated in Fig. 5(c). If step down is less than 0.15mm or greater than 0.5mm, the steel/aluminum alloy sheets are difficult to be bonded. If wall angle is greater than 65° , the part is easy to crack. If wall angle is less than 45° , the part is also difficult to be bonded. If step down is in a small scope of 0.15-1.25mm, interaction between wall angle and step down has insignificant effect on maximum peeling force.

When the other parameters are fixed, as step down δ increases, the peeling force shows a trend close to monotonous increasing, which is mainly because it affects the

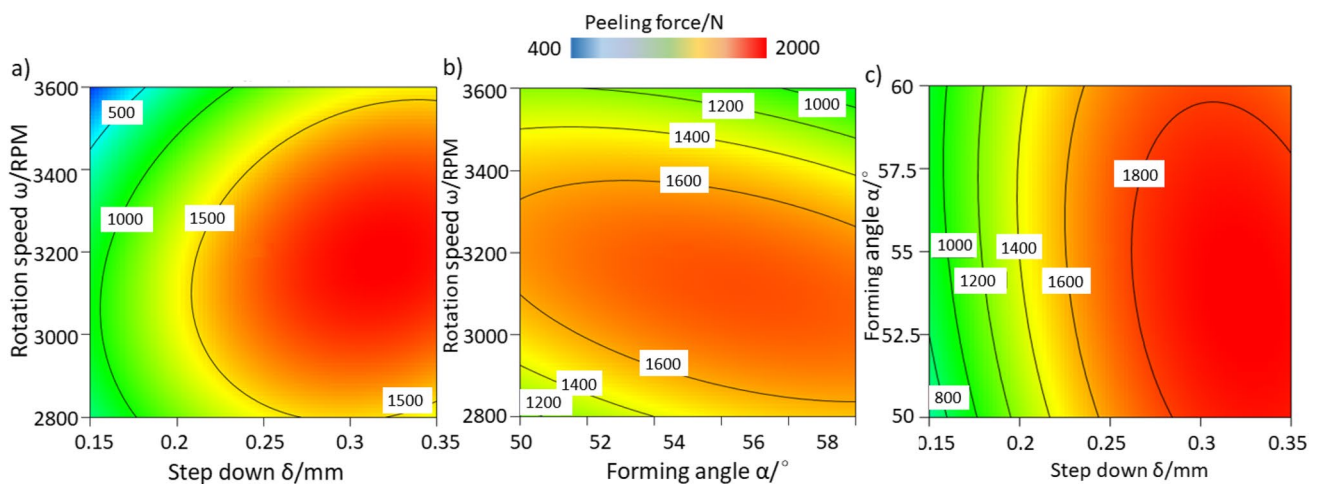


Fig. 5 The interaction effects of cross terms of process parameters on peeling force: (a) step down δ and rotation speed of MT ω , (b) forming angle α and rotation speed of MT ω , (c) step down δ and forming angle α

amount of deformation, heat conduction and forming force during the process. Larger step down will result in more severe local plastic deformation of the sheets, which may promote atoms fast diffusion at the interface. However, if step down is too large, the accumulated heat will be reduced due to shorter forming time.

The wall angle α shows unapparent individual effect on the maximum peeling force when the other parameters are fixed. Wall angle shows weak effect on bonding strength. Because wall angle mainly affects the plastic work and the thickness distribution of the sheets during the process, which may contribute less in heat generation. It is found that if the wall angle is less than 45° , the dissimilar sheets are difficult to be bonded, and if wall angle is greater than 65° , the thickness of the part is greatly reduced.

As rotation speed of MT ω increases, the maximum peeling force firstly increases and then decreases when the other parameters are fixed. During the process, the rotational MT produces adequate frictional heat in the contacted surface of metallic sheet. Generally, higher rotation speed will bring more frictional heat, which is beneficial to bonding strength. After reaching the peak stage, the frictional heat generation at the rounded corners decreases due to skidding and the bonding quality decreases.

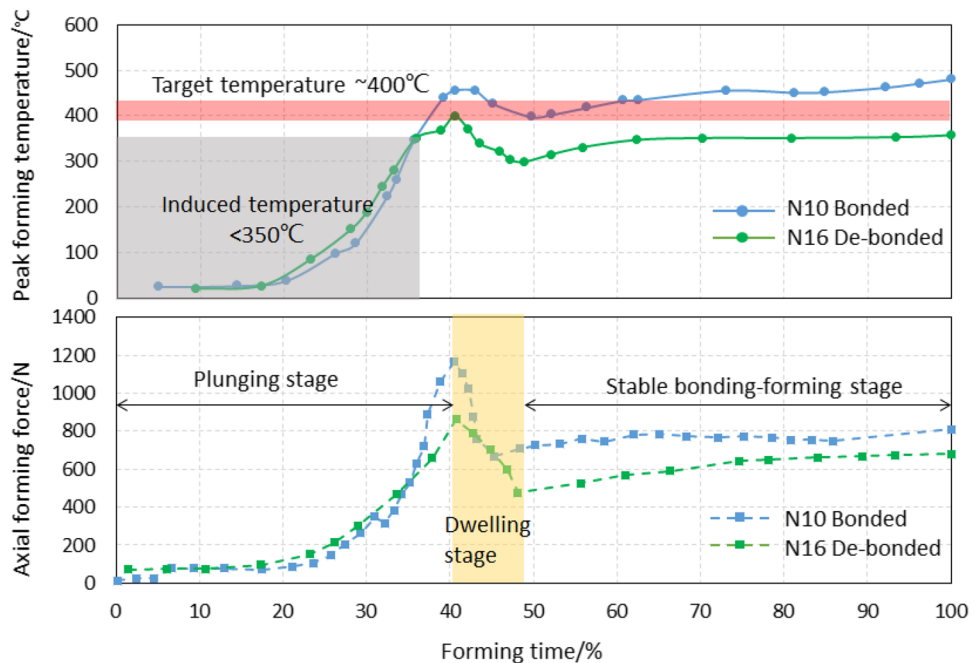
Therefore, the reasonable process window could be derived as $0.4\text{mm} > \delta > 0.2\text{ mm}$, $60^\circ > \alpha > 50^\circ$, $3600\text{ RPM} > \omega > 3000\text{ RPM}$.

Effects of forming force and working temperature on interfacial bonding

Axial forming force and working temperature in loading area are of great interest, which are the direct indicators of working states. As displayed in Fig. 6, the history records of axial forming force and working temperature are in a similar trend. Moreover, high axial forming force will cause strong friction stir effect, then working temperature in the loading area is correspondingly elevated. The temperature variation in all experiments is similar. In the initial stage, working temperature gradually rises with heat accumulation. When the forming depth reaches 5mm, the working temperature and forming force decrease due to materials softening. Afterwards, the process tends to stabilize. Within the balance of heat generation and conduction between the sheets and other machine configurations, working temperature and axial forming force rise slowly and gradually stabilize at around 400°C and 800 N at stable bonding-forming stage, respectively.

If working temperature is lower than 350°C , steel/Al sheets cannot be bonded (i.e., NB mode). Because the low steady-state temperature and pressure will not promote effective fast diffusion between the dissimilar interfaces, and the generated weak mechanical bonding can only result in unstable laminated structure. From the experimental data plotted and fitted in Fig. 7, the tests indicate that the peeling force increases with the increase of temperature in the temperature range of $300 - 450^\circ\text{C}$. But a further increase in temperature ($\geq 500^\circ\text{C}$) may cause fusion welding and result in formation of thick-brittle

Fig. 6 The peak temperature and axial force history of forming tests N10 and N16



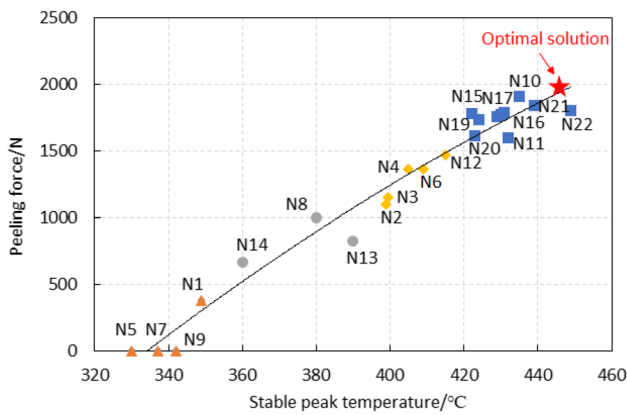


Fig. 7 The peeling force versus stable peak temperature

IMCs, which seriously reduces the bonding strength. Cracking and excessive thinning are harmful to the bonding strength of part, and it will tear from the base material during the peeling test (i.e., PS mode). Therefore, a quadratic function can be obtained by considering the relationship between working temperature T and peeling force y . The experimental points are shown in Fig. 7 and the fitting model with R^2 equaling to 0.9675 is represented as,

$$y = -0.033T^2 + 43.194T - 10742 \quad (300 < T < 500) \quad (5)$$

Performance evaluation within process window

Ultimate forming depth

During this thermomechanical process, the sheet metal formability can be effectively increased even compared to pre-prepared steel/Al laminates [30]. A few promoting procedures are employed like pre-heat (~150 °C) and low rotation speed of ST (300 RPM) to obtain higher formability. The modified solution can promote material flow with relative low heat-force and inhibit the stress triaxiality of loading area. Under the action of local compressive stress applied by the rigid tools, the damage caused by micro holes in loading area is suppressed so that large forming depth can be obtained [31]. In the derived optimal solution of the FS-DSIF&SB process, ultimate forming depth as a simple formability metric can be used. As shown in Fig. 8, the laminates can be formed to 45mm without cracking in the design of part with fixed wall angle of 53°. In the design of part with variable wall angle, cracks occur at 45mm of forming depth. The formability of part needs further quantitative analysis to understand the interfacial behaviors.

Apart from the high formability of FS-DSIF&SB process, proper thickness thinning rate is also a great concern for a conical part with variable wall angle as shown in Fig. 9. The cross section is cut from the meridian direction to show the interfacial bonding state and thickness distribution after the forming process. Thickness distribution at forming depth 25mm is also illustrated here.

The requirement on proper process parameters combination is attributed to stable forming force. Uniform wall thickness distributions in both DC05 and AA5052 sides shall

Fig. 8 The fabricated laminated parts with different shape design



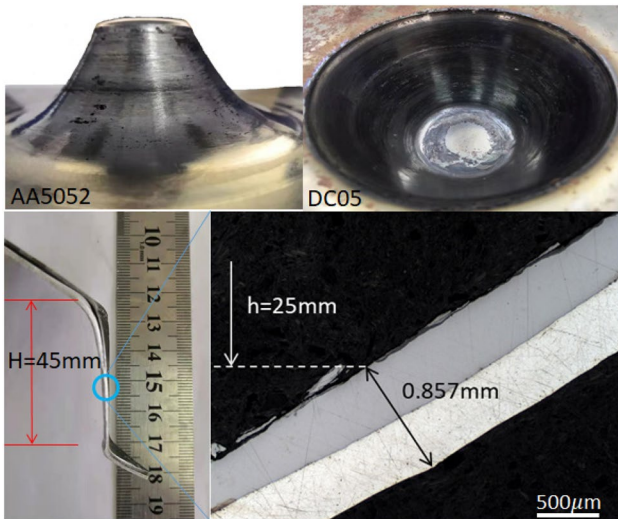


Fig. 9 The view of a part with variable wall angle and its sidewall appearance

be achieved to improve service performance. From the measured results as shown in Fig. 10, the thickness distribution fails to follow the cosine law which is commonly valid in most ISF processes [32]. When the forming depth reaches 25 mm, the thickness of laminates is severely reduced to 0.857mm (0.555mm in AA5052 sheet, 0.302mm in DC05

Fig. 10 The wall thickness variation along with the forming depth

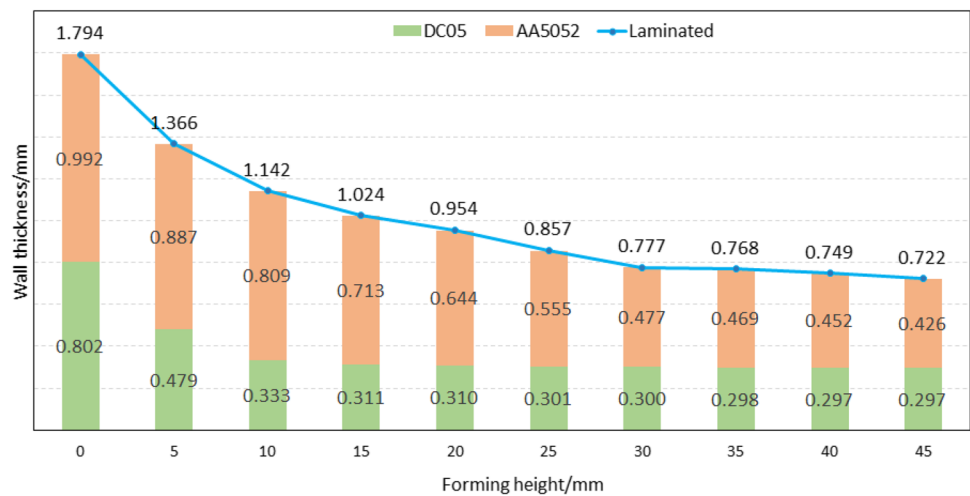
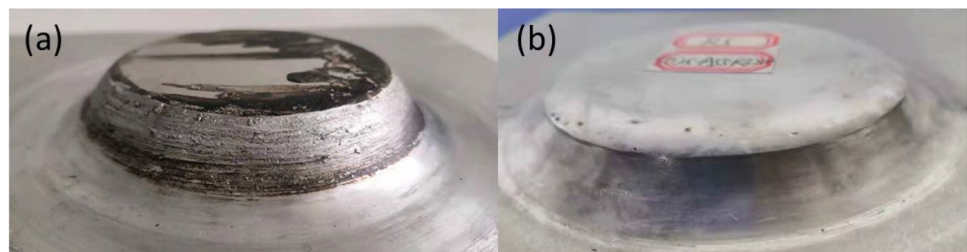


Fig. 11 The influence of grease on the surface quality of AA5052 surface of truncated cone: (a) drop point 598°C, (b) drop point > 800°C



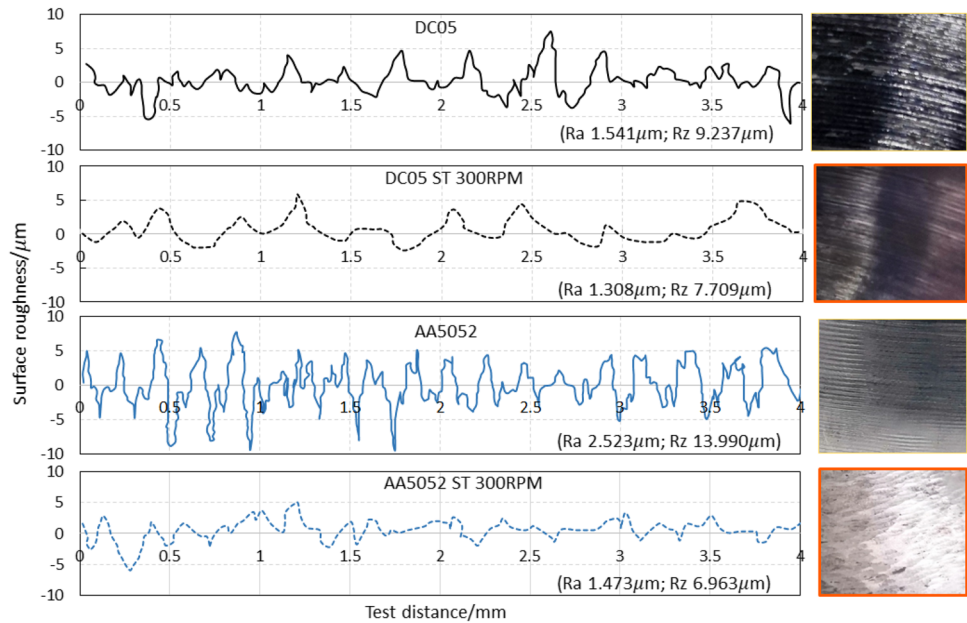
sheet), nearly 50% of initial value. Especially when the forming depth is less than 20mm, the total thickness decreases rapidly due to the squeezing effect of rigid tools. Because low heat accumulation in the initial process stage may hardly affect the plastic deformation resistance of the materials, the thickness change is mainly affected by the geometric shape. However, as the cutting and soften effects are obvious in following processing stages, the thickness is mainly controlled by squeezing factor of rigid forming tools.

Surface finish

The tools with high-speed rotation generated the friction heat to cause the sheets to soften during the process with localized cyclic heating. Friction stir with axial force in local loading area may result in cutting effect on material surface which is harmful to the surface quality, especially the softer aluminum alloy side. In order to ensure the surface finish quality of the AA5052 surface, it takes a qualitative leap by selecting grease with higher drop point. The results of trial-error experimental tests are shown in Fig. 11. Therefore, high-temperature resistant graphite grease shall be employed during FS-DSIF&SB process.

As illustrated in Fig. 12, the phenomenon of onion circle appears in the surfaces of parts. The milling effect of MT certainly reduces the surface quality of DC05, and can be

Fig. 12 Finished surface roughness of DC05 and AA5052 sides



solved by larger arc radius of MT. Compared with original process, it can be found that the rotational ST has a significant effect on smoothing the surface roughness, R_a of the steel and Al side is reduced by about 15.12% and 41.62%, respectively. Because rolling friction can effectively avoid excessive tangential forces leaving “furrows” on the AA5052 surface. Few aluminum alloy chips adhere to ST during FS-DSIF&SB process.

Conclusions

In the present work, a novel friction stir assisted dissimilar bonding with double-sided incremental forming process is used to fabricate truncated steel/Al laminated parts, and a series of peeling tests are conducted to reveal the effects of main process parameters. The main conclusions are summarized as follows.

- (1) The dominated independent parameters of the ISF-FSW combined process are in a sequence of step down δ , wall angle α , rotation speed of master tool ω . Among the cross terms, the combined effect of rotation speed of master tool and wall angle is dominated.
- (2) The derived process window for better high bonding strength is determined as $0.4\text{mm} > \delta > 0.2\text{ mm}$, $60^\circ > \alpha > 50^\circ$, $3600\text{ RPM} > \omega > 3000\text{ RPM}$. Maximum peeling force as 1925 N can be obtained with optimal process parameter set as $\delta = 0.323\text{mm}$, $\alpha = 53.4^\circ$, $\omega = 3210\text{RPM}$.
- (3) Increased temperature and axial forming force are beneficial to interfacial bonding. Temperature and bonded

strength are positively correlated within the scope of $300 - 450^\circ\text{C}$. If the temperature is lower than 350°C , the dissimilar sheets cannot be successfully bonded.

- (4) With the optimal parameter combination, forming depth of conical part as simple metric of formability in ISF-related process can reach 45mm at a fixed wall angle 53° without crack. Uniform thickness distribution can be obtained during the process. Slave tool with low rotation speed 300RPM can also effectively improve the surface quality.

Acknowledgements The authors are grateful for the funding of National Natural Science Foundation of China under grants # 51675332 and Program of Shanghai Excellent Academic Research Leadership (19XD1401900).

Declarations

Conflict of interest The authors declare absence of any conflict of interests.

References

1. Woo YY, Oh IY, Hwang TW, Moon YH (2019) Analysis of shape defects during flexible roll forming of steel/aluminum double-layered blanks. *Int J Mater Form* 13(6):861–872
2. Ma Y, Lou M, Li Y, Lin Z (2018) Effect of rivet and die on self-piercing rivetability of AA6061-T6 and mild steel CR4 of different gauges. *J Mater Process Technol* 251:282–294
3. Tanaka T, Morishige T, Hirata T (2009) Comprehensive analysis of joint strength for dissimilar friction stir welds of mild steel to aluminum alloys. *Scrip Mater* 61(7):756–759

4. Ma Y, Yang B, Lou M, Li Y, Ma N (2020) Effect of mechanical and solid-state joining characteristics on tensile-shear performance of friction self-piercing riveted aluminum alloy AA7075-T6 joints. *J Mater Process Technol* 278:116543
5. Zhang S, Wang W, Ma S, Yan H, Jiao L, Li Q (2020) A solid state bonding technology for metal plate by shear-extrusion and the analysis of microstructure and bonding strength. *J Manuf Process* 59:477–486
6. Yuan L, Xiong J, Peng Y, Li Z, Li J (2020) Modeling void closure in solid-state diffusion bonding of TC4 alloy. *Vacuum* 173:109120
7. Zhang JY, Xu B, Haq Tariq N, Sun M, Li D, Li YY (2020) Microstructure evolutions and interfacial bonding behavior of Ni-based superalloys during solid state plastic deformation bonding. *J Mater Sci Technol* 46:1–11
8. Abe Y, Kato T, Mori K (2008) Self-pierce riveting of three high strength steel and aluminium alloy sheets. *Int J Mater Form* 1:1271–1274
9. Mishra RS, Ma ZY (2005) Friction stir welding and processing. *Mater Sci Eng: R* 50(1):1–78
10. Liu FC, Dong P (2021) From thick intermetallic to nanoscale amorphous phase at Al-Fe joint interface: roles of friction stir welding conditions. *Scrip Mater* 191:167–172
11. Bakavos D, Chen Y, Babout L, Prangnell P (2011) Material interactions in a novel pinless tool approach to friction stir spot welding thin aluminum sheet. *Metal Mater Trans A* 42(5):1266–1282
12. Kuang B, Shen Y, Chen W, Yao X, Xu H, Gao J (2015) The dissimilar friction stir lap welding of 1A99 Al to pure Cu using Zn as filler metal with “pinless” tool configuration. *Mater Des* 68:54–62
13. Leon MD, Shin HS (2015) Material flow behaviours during friction stir spot welding of lightweight alloys using pin and pinless tools. *Sci Technol Weld Join* 21(2):140–146
14. Leitao C, Louro R, Rodrigues DM (2012) Analysis of high temperature plastic behaviour and its relation with weldability in friction stir welding for aluminium alloys AA5083-H111 and AA6082-T6. *Mater Des* 37:402–409
15. Zhao W, Wu C, Su H (2020) Numerical investigation of heat generation and plastic deformation in ultrasonic assisted friction stir welding. *J Manuf Process* 56:967–980
16. Liu X, Wu C, Padhy GK (2015) Characterization of plastic deformation and material flow in ultrasonic vibration enhanced friction stir welding. *Scrip Mater* 102:95–98
17. D’Urso G, Giardini C (2015) FEM model for the thermo-mechanical characterization of friction stir spot welded joints. *Int J Mater Form* 9(2):149–160
18. Jackson K, Allwood J (2009) The mechanics of incremental sheet forming. *J Mater Process Technol* 209(3):1158–1174
19. Emmens WC, Sebastiani G, Boogaard A (2010) The technology of incremental sheet forming—A brief review of the history. *J Mater Process Technol* 210(8):981–997
20. Cerro I, Maidagan E, Arana J, Rivero A, Rodriguez PP (2006) Theoretical and experimental analysis of the dieless incremental sheet forming process. *J Mater Process Technol* 177(1–3):404–408
21. Lu B, Fang Y, Xu DK, Chen J, Ai S, Long H, Ou H, Cao J (2015) Investigation of material deformation mechanism in double side incremental sheet forming. *Int J Mach Tool Manuf* 93:37–48
22. Xu DK, Lu B, Cao TT, Chen J, Long H, Cao J (2014) A comparative study on process potentials for frictional stir- and electric hot-assisted incremental sheet forming. *Proce Eng* 81:2324–2329
23. Wang ZH, Cai S, Chen J (2019) Experimental investigations on friction stir assisted single point incremental forming of low-ductility aluminum alloy sheet for higher formability with reasonable surface quality. *J Mater Process Technol* 277:116488
24. Ambrogio G, Filice L, Gagliardi F (2012) Formability of lightweight alloys by hot incremental sheet forming. *Mater Des* 34:501–508
25. Matsumoto R, Sakaguchi H, Otsu M, Utsunomiya H (2020) Plastic joining of open-cell nickel foam and polymethyl methacrylate (PMMA) sheet by friction stir incremental forming. *J Mater Process Technol* 282:116691
26. Li M, Wu RH, Cai S, Chang Z, Wang Z, Chen J (2020) Experimental investigation on friction-stir-assisted incremental forming with synchronous bonding of aluminum alloy and steel sheets. *J Mater Eng Perform* 29(2):750–759
27. Wu RH, Li M, Liu X, Cai S, Chen J (2020) Characterization of material flow in friction stir-assisted incremental forming with synchronous bonding of dissimilar sheet metals. *Int J Adv Manuf Technol* 109(9–12):2523–2534
28. Cai S, Wu RH, Wang Z, Li M, Chen J (2020) Numerical simulation of friction stir-assisted incremental forming with synchronous bonding of heterogeneous sheet metals. *Int J Adv Manuf Technol* 106(7–8):2747–2763
29. Honarpisheh M, Jobedar MM, Alinaghian I (2018) Multi-response optimization on single-point incremental forming of hyperbolic shape Al-1050/Cu bimetal using response surface methodology. *Int J Adv Manuf Technol* 96(9–12):3069–3080
30. Abd R, Chen W, Jin K, Bao Y, Hussein AW (2019) Formability and failure analyses of Al/SUS bilayer sheet in single point incremental forming. *Int Adv Manuf Technol* 105(7–8):2785–2798
31. Wu RH, Liu XM, Li M, Chen J (2021) Investigations on deformation mechanism of double-sided incremental sheet forming with synchronous thermomechanical steel-aluminum alloy bonding. *J Mater Process Technol* 294:117147
32. Ai S, Lu B, Chen J, Long H, Ou H (2017) Evaluation of deformation stability and fracture mechanism in incremental sheet forming. *Int J Mech Sci* 124–125:174–184

Publisher’s Note Springer Nature remains neutral with regard to jurisdictional claims in published maps and institutional affiliations.